Available Online

JSR Publications

J. Sci. Res. **13** (3), 961-969 (2021)

JOURNAL OF SCIENTIFIC RESEARCH

www.banglajol.info/index.php/JSR

Influence of Cobalt Substitution in $LaNiO_3$ Nanoperovskite on Catalytic Propylene Oxidation

T. Vaz[1*], S. M. Gurav[2], A. V. Salker[3]

[1]Department of Chemistry, St. Xavier's College, Mapusa, Goa, 403507, India

[2]Department of Chemistry, Government College of Arts, Sc., and Com, Quepem, Goa, India

[3]School of Chemistry, Goa University, Goa 403206, India

Received 14 March 2021, accepted in final revised form 13 May 2021

Abstract

Perovskite-type oxides with transition elements offer promising potential as catalysts in total oxidation reactions. The present work reports the synthesis of crystalline lanthanum nickelates and cobaltates and their intermediate nanomaterials compositions $LaNi_{1-x}Co_xO_3$ (x = 0.3, 0.5, and 0.7) at 800 ºC by co-precipitation precursor technique for structural, morphological, and total propylene oxidation catalytic activity. The evolution of the crystal structure and formation of the perovskite phase were analyzed by X-ray diffraction, Thermo Gravimetry Analysis (TGA) / Differential Scanning Calorimetry (DSC), Fourier Transformed Infra-Red (FTIR), Atomic Absorption Spectroscopy (AAS), Scanning Electron Microscopy (SEM), Brunauer–Emmett–Teller (BET), Electron Spin Resonance (ESR) techniques. The terminal compounds $LaNiO_3$, $LaCoO_3$, and their intermediates compositions were identified to be single-phase and are indexed to rhombohedral structures. The bonding characteristics were studied by FTIR spectroscopy. On substitution of Ni with Co in B-site, the slight distortion in XRD diffraction peaks were observed. These compounds show a considerable increase in the activity of propylene oxidation to carbon dioxide. This study aims at understanding the effect of B– site substitution in the lattice of $LaNiO_3$ and their influence on catalytic propylene oxidation efficiency.

Keywords: Rare earth perovskites; Co-precipitation; Catalytic oxidation; Propylene.

© 2021 JSR Publications. ISSN: 2070-0237 (Print); 2070-0245 (Online). All rights reserved.
doi: http://dx.doi.org/10.3329/jsr.v13i3.52435 J. Sci. Res. **13** (3), 961-969 (2021)

1. Introduction

The perovskite-type $LaBO_3$ (B = transition element) presents very interesting physical properties. They exhibit an array of applications in microelectronics, conductive electrodes, micro-actuators, piezoelectric energy harvesters, magneto electronics, sensors, magnetic memory devices, solar cells and as catalysts [1-6]. The Ln ions support the framework, stabilizes the system. Hence, the size of these ions defines the octahedral structural transformations, which decide the physical properties, govern the electronic state and the phase transition. A perovskite-type mixed metal oxide with ABO_3 structure,

* *Corresponding author*: teovaz18@gmail.com

wherein the cation with larger radius is coordinated to 12 oxygen atoms and occupy A-, and B-sites. A and O form the closest cubic packing, and B occupy octahedral voids in the lattice. The substitution of A- and/or B-site with different metal ions having various sizes and charges, shows great structural flexibility, altering the electronic properties and resulting to fascinating large-scale applications. While the robust structure of these oxides capable of accommodating a large number of metals to improve the quality of materials, offering high possibilities space for catalysis [7]. Catalytic combustion provides one of the most effective means of controlling automobile pollution. Compared with presently in use noble metal, other metal oxide catalysts offer sufficient activity and thermal stability as oxidation catalysts, having advantages of economic viability and potential usage in the energy-generating systems and a promising candidate for an auto exhaust catalyst [8].

In general, a large number of elements can be obtained as ideal cubic or modified perovskites structures depending upon their tolerance factor. The ideal structure was mostly successful for a tolerance factor close to 1 and at suitable temperatures. In other conditions, preferred distortions orthorhombic, rhombohedral, and to a lesser extent tetragonal, mono, or triclinic perovskites will appear [8]. Although, it is difficult to synthesize these materials in their pure bulk form, due to the stabilization of Ni(III) and either oxygen pressure and/or high temperatures of ~950 ºC are necessary [1,2,8,9], it is possible to prepare these perovskite materials comparatively in the pure form either by modified conventional ceramic, co-precipitation, sol-gel, hydrothermal, auto-combustion and also by other modern techniques like pulse laser, spray pyrolysis techniques for thin films. $LaNiO_3$ and $LaCoO_3$ have rhombohedrally distorted perovskite structures at room temperature [3,4,9-11].

Metal oxides catalyze the oxidation of propylene with oxygen giving rise either to partial (selective) or total oxidation to CO_2. The total oxidation of propylene with the aim of reducing air pollutants is an important consideration in terms of automobile and industrial pollution control. Several investigators have studied the solid-state and the catalytic activity of propylene oxidation over several $LaBO_3$ compounds. Their studies have shown that the non-noble metal-containing $LaBO_3$ catalysts are chemically active species for total hydrocarbon oxidation [12-14]. In the present study, an attempt is made to understand the effect of B-site substitution of Ni atom by cobalt in the lattice of $LaNiO_3$, its influence, and the comparative catalytic activity of the progressively substituted $LaNiO_3$ with various cationic compositions prepared by co-precipitation precursor technique, in the oxidation of propylene and their correlation with the structural properties.

2. Materials and Methods

2.1. *Co-precipitation hydroxide precursor synthesis*

The perovskite-type compositions of $LaNi_{1-X}Co_XO_3$ were synthesized by co-precipitation precursor technique at 800 ºC as discussed elsewhere [15]. Stoichiometric quantities of

hydrated salts $La(NO_3)_3$, Ni/Co nitrates (AR) were dissolved together in a minimum quantity of distilled water. Aqueous solutions were mixed on a magnetic stirrer and slowly precipitated, adding 5 % sodium hydroxide solution. The precipitate obtained was digested for 15 min and the resultant precipitate mixture was subjected to oxidation using 6 % H_2O_2 solution. It was allowed to set overnight. The hydroxide precursor precipitate was then washed, filtered, and dried in an oven at 150 ºC. A small portion of it was preserved for TG/DSC analysis. The dried precipitate was homogenized well in an agate mortar and further heated at 300, 600, and finally at 800 ºC in the air for a total time of 10-12 h. The furnace-cooled compositions were stored in the air-tight containers for characterization and for further propylene oxidation.

2.2. *Material characterization*

Thermal gravimetric analysis (TGA) / differential scanning calorimetry (DSC) was carried out on a representative hydroxide precursor, using NETZSCH - Garetebau GmbH Thermal Analyzer, to check the optimum temperature required to complete the perovskite phase. The system compositions were characterized by X-ray powder diffraction technique with Rigaku Miniflex tabletop instruments, using Cu Ka, filtered through Ni absorber. Shimadzu FTIR instrument (model 8101A) was used to record FTIR spectra. The sodium impurity in the perovskite materials prepared by the co-precipitation method using sodium hydroxide was found by employing atomic absorption spectroscopy (AAS). The specific surface areas were measured using the BET nitrogen adsorption method (QUANTACHROME NOVA 1200 version 3.70). The perovskites containing paramagnetic species and the identification of the catalytically active species for the reaction were checked with ESR study. The ESR spectra were recorded at the X-band on a Varian E-112 spectrophotometer at liquid nitrogen temperature. Tetracyanoethylene was used as a field calibrant with its g-value as 2.00277 and the sample was mounted on a quartz tube. The hysteresis behavior to evaluate the saturation magnetization was studied on a selected magnetic sample using a high field hysteresis loop tracer. The saturation magnetization values, σs in emu/g, of some magnetic perovskite samples were measured.

Total propylene oxidation was studied as a model test reaction using oxygen in nitrogen with a continuous flow, fixed bed quartz reactor by placing 1 g of powdered nano-catalyst in between glass wool plugs. The catalyst activity was determined using a feed gas composition of 5 % propylene, 5 % O_2 in nitrogen. The flow rates of individual gases were controlled by flow meters and precision needle valves. The products and the feed gases were analyzed using an online gas chromatograph with a Porapak N and molecular sieve 13X columns. H_2 was used as a carrier gas. The propylene, oxygen, and nitrogen gases were used from pure commercially available cylinders, purified further by passing through a molecular sieve and alkali traps [15].

3. Results and Discussion

TG/DSC was recorded to study the behavior of weight loss of the hydroxide precursor. Fig. 1 displays a typical TG-DSC curve of selected $LaNiCo(OH)_6 \cdot xH_2O$ precursor from r. t. to 900 ºC. The powdered form of a precursor (approx. 20 mg) was placed in an alumina crucible, covered with a lid, and continuously weighed as it is heated at a constant linear rate of 10 ºC/min. An endothermic event centered at 104 ºC was the usual loss of moisture from the precursor, and a negligible mass loss in the TG curve was observed. The weight loss of 8.45 % between r.t. and 275 ºC was observed due to the loss of moisture. The combined decomposition of $LaNiCo(OH)_6.xH_2O$ hydroxides was observed in the range of 275 to 400 ºC. Further, the decomposition of hydroxides and observed linear weight loss is due to initiation of solid-state diffusion together with weight loss of 9.97 % and perovskite phase formation between 400-800 ºC in agreement with the literature [16].

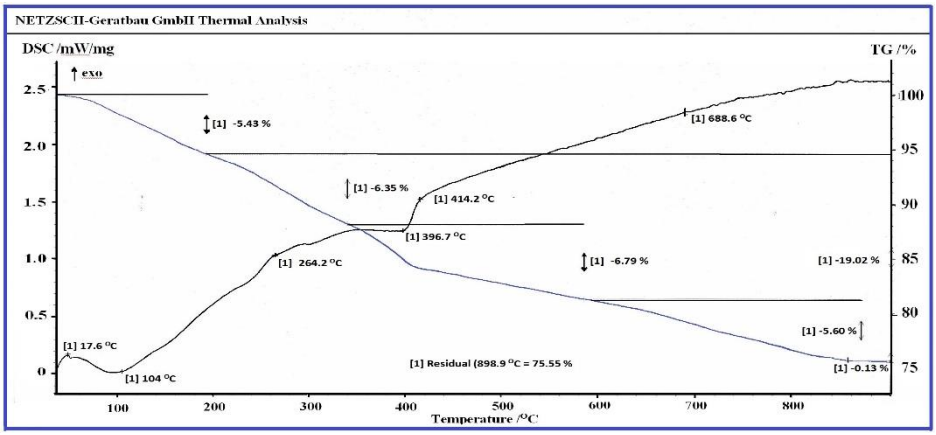

Fig. 1. TG/DSC curves for $LaNiCo(OH)_6.xH_2O$ precursor.

The crystal structure of prepared perovskite nanomaterials was investigated by X-ray powder diffractograms. The d_{hkl} and 2θ values obtained from the characteristic reflections were compared with the values reported in the literature (JCPDS data file). Since the d_{hkl} value of the intermediate compositions is not reported, the values were compared with the end compositions. Fig. 2 shows XRD patterns for $LaNiO_3$, $LaNi_{0.5}Co_{0.5}O_3$, and $LaCoO_3$, calcined at a final temperature of 800 ºC. It is observed that at 600 ºC, the perovskite phase formation is incomplete, as impurity peaks of respective metal oxides are prominent.

Our results of X-ray analysis showed that the $LaNi_{1-X}Co_XO_3$ system compositions, heated at 800 ºC can be clearly indexed to be rhombohedrally distorted perovskites, in accordance to JCPDS file 34-1181 and 48-0123 for $LaNiO_3$ and $LaCoO_3$, respectively. The general appearance of the diffractograms remains similar, as all the compositions belong to the same crystal structure family. It may be interesting to observe that the diffraction

angles remain the same for all intermediates, with only minor changes in the intensity due to Ni/Co ratio. The observed characteristic splitting in the diffraction peaks is evidence of the rhombohedral distortion of the perovskite structure [17]. The average crystallite particle sizes calculated from the four intense diffraction peaks data using Debye Scherrer's formula were in the range of 10.2 nm and 44.3 nm, confirming their nano-crystalline nature of materials.

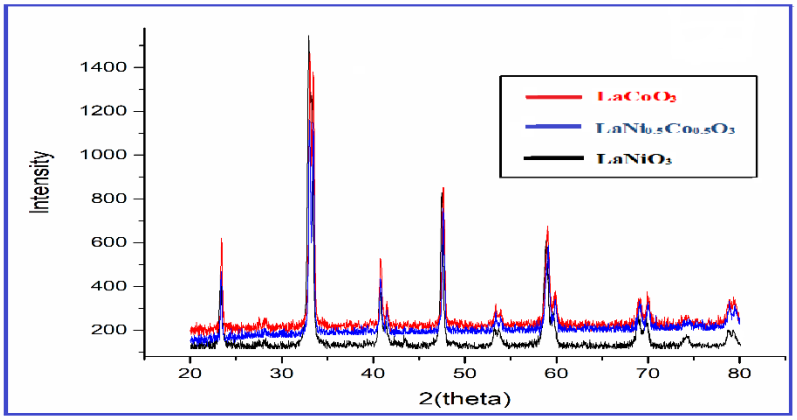

Fig. 2. XRD pattern of $LaNiO_3$, $LaNi_{0.5}Co_{0.5}O_3$, and $LaCoO_3$ materials.

The sodium contamination was estimated using an AAS and found to be in the range of 0.2 to 0.4 % by weight. Surface areas obtained by BET nitrogen adsorption method were found to be in the range of 3.9 - 20.4 m^2/g for these nanomaterials.

FTIR spectra in the region 1000 to 300 cm^{-1}, can be used to characterize the perovskite structure [18]. In the IR spectra of perovskites, two strong characteristic absorption bands were observed in the 700 to 390 cm^{-1} region corresponding to the stretching vibration of the M-O bond. The lower absorption band has been attributed to a deformation mode of MO_6 (B= Ni or Co) octahedral. i.e., the bond angles of B-O-B in the perovskite structure. The FTIR spectrum of the $LaNiO_3$ compound does not show any feature characteristic of localized vibration modes, which is peculiar of the $LaNiO_3$. The vibrational modes disappear for the compounds having very low resistivity, as in the case of $LaNiO_3$. It is observed that with the substitution of Co^{+3} in $LaNiO_3$, the strong absorption peak at 593 cm^{-1} gets gradually broadened for compositions from x = 0.3 to x = 0.7 and shift to a higher frequency. The FTIR spectra for x = 0.3, 0.5, and 0.7 show similar patterns, whereas, for $LaCoO_3$, distorted shouldered peaks at 600 and 570 cm^{-1} were observed, which indicate marginal structural symmetry change [18].

In Fig. 3a, micrograph of $LaNiO_3$, no clear particle structure, but granular spherical nanoparticles agglomeration was observed. In Fig. 3b, the spherical particles have become distinct and $LaCoO_3$, as observed in Fig. 3c a clear spherical-shaped structure, is prominent. The particle size was observed in the range of 47 to 98 nm on an average of the nanosystem materials. Significant changes in the morphology are observed when B-

site Ni is substituted with more oxyphilic Co atoms, promoting the formation of better spherical shaped particles having higher porosity. It was noted that $LaCoO_3$ nanoparticles were comparatively in a smaller size in the range of 58 to 69 nm.

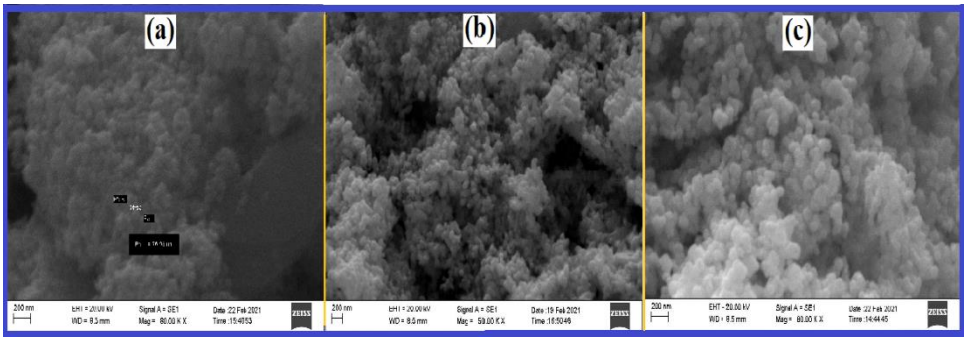

Fig. 3. SEM images of a) $LaNiO_3$ b) $LaNi_{0.5}Co_{0.5}O_3$, and c) $LaCoO_3$ materials.

While these compounds did not show any ESR spectra at r.t., they showed broad spectra at liquid nitrogen (N_2). Fig.4 shows ESR spectra of different perovskites at liquid N_2 temperature. For heavier atoms like La^{+3}, the spin-orbit coupling is strongly coupled to lattice vibrations and spin relaxation time; therefore, it is very small at high temperatures. This means that ESR spectra too broad to be detected even at r. t.

The observed g-values were 3.8, 4.8, 5.2, 5.8 emu/g for x = 0, 0.3, 0.5, and 0.7 compositions respectively, and are found to increase with increase in 'x' value. For $LaCoO_3$, the g-values of 3.7 emu/g were observed. A very weak ESR signal with broad line width was observed only at liquid nitrogen temperature for $LaNi_{1-X}Co_XO_3$, giving an indication that Ni^{+3}, Co^{+3} ions are ESR inactive [19].

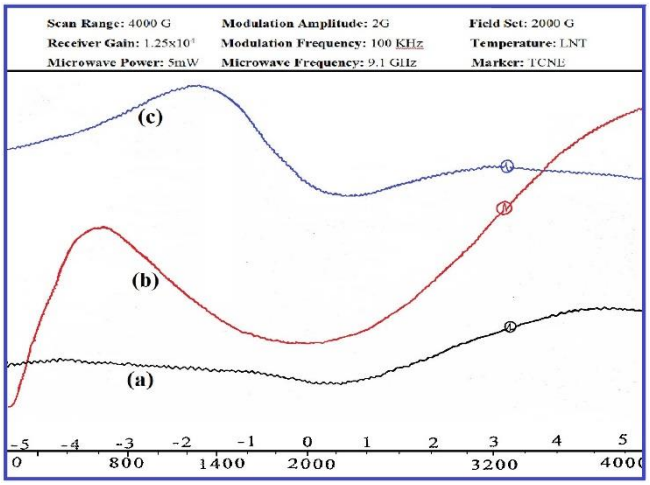

Fig. 4. ESR plots of a) $LaNiO_3$ b) $LaNi_{0.5}Co_{0.5}O_3$, and c) $LaCoO_3$.

The temperature dependence of propylene oxidation studies on different compositions of the $LaNi_{1-X}Co_XO_3$ system is shown in Fig. 5. The results showed some interesting trends of activity. Both terminal compounds showed low activity up to 225 ºC, and higher conversion of around 90-92 % at about 475 ºC. Incorporation of Co in the $LaNiO_3$ lattice showed a significant rise in the catalytic activity below 225 ºC, and there was no sharp rise in activity further above 300 ºC for propylene oxidation. It was also observed that all the compositions showed 60-65 % conversion at around 325 ºC. The oxidation activity was maximum for x = 0.7 composition, followed by x = 0.5, 0.3, 1.0. $LaNiO_3$ showed comparatively low oxidation capacity up to 325 ºC. For the end compositions $LaNiO_3$, x = 0.5, and $LaCoO_3$, the induction temperature was 75 ºC, which was 50 ºC higher than for the intermediates.

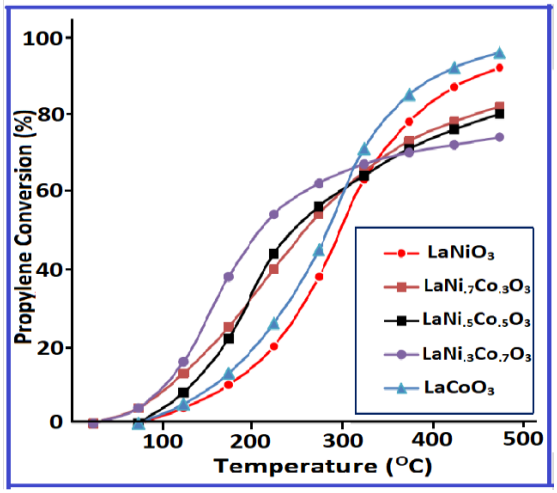

Fig. 5. Catalytic propylene oxidation on $LaNi_{1-X}Co_XO_3$ system.

The mechanism of heterogeneous catalytic oxidations essentially involves interaction between a hydrocarbon and surface-active oxygen. The chemisorption of O_2 and total oxidation of propylene on $LaBO_3$ perovskites are interrelated. The catalytic activity increases in the same order of the adsorption of O_2 on a clean surface. Thus, $LaCoO_3$, having considerably higher adsorption of O_2 showed better activity than $LaNiO_3$ for the total oxidation. Further, the activation energy for $LaCoO_3$ is lower than $LaNiO_3$. In $LaBO_3$ perovskite-type of oxides, B- ions are situated in the center of an octahedron, whose vertices are occupied by O ions and the B-O bond strength differs from each member of the transition series, depending upon their tolerance factor. Therefore, under the condition of adsorption and catalysis, different surface defect concentrations and nature may be produced in each of these oxides. The change in crystal field stabilizes energy due to the change in the co-ordination number of B^{+3} ions on adsorption of O_2 and their experimental profiles of adsorption and catalysis [20]. Thus, the relationship between the local

symmetry of surface cations, the adsorption, and catalysis, shows the importance of localized interactions in these surface processes.

On the other hand, the observed relation between the catalytic activity for the total oxidation and the O_2 adsorption shows that the adsorbed O_2 (not the lattice O_2) plays an important role in this catalytic reaction. This indicates that the total oxidation of propylene occurs through the suprafacial catalysis mechanism, in which the catalyst provides orbitals of appropriate energy and symmetry for the bond formation with the reactant and intermediate. The O_2 adsorption and the total oxidation of propylene on $LnCoO_3$ are attributed to the activation energy and the bond strength of propylene, with the adsorbent surface greatly influencing the catalytic action for oxidation by these perovskite materials [21].

In the case of $LaCoO_3$, the B- site Co^{+3} has $t_{2g}^6e_g^0$, whereas, in $LaNiO_3$, the B-site has $t_{2g}^6e_g^1$ orbital occupation and the t_{2g} levels are completely filled. As the substitution of Ni by Co increases in the $LaNiO_3$ lattice, Co^{+3} ions must be providing empty e_g^0 orbitals for O_2 adsorption, which influences the suprafacial mechanism for the total oxidation of propylene. As the substitution of Ni^{+3} by Co^{+3} ions in the $LaNiO_3$ lattice, the transition of electron spin density to the empty, e.g., levels of Co^{+3} ions increases. As a result, the O_2 adsorption becomes less, thereby gradually decreasing the propylene oxidation, as seen in Fig. 2. Further, the superior conversion shown by intermediates may be due to the arising of the strong synergistic effect of mixing of B-sites, even when the host and the substitute cations have the same valency [22]. Such substitution led to defect structures, which is evident from the diffraction peak splitting observed in the XRD plots. The probable explanation for the enhancement of catalytic activity for the intermediate compositions up to 325 ºC may be due to the cooperative (synergistic) effect of Ni^{+3} and Co^{+3} ions in the B- site and observed high surface areas leading to the increased O_2 adsorption. The decrease in activity, with further increase in the temperature, may be due to the non-availability of enough O_2 for the oxidation reaction above 325 ºC.

4. Conclusion

Crystalline $LaNi_{1-X}Co_XO_3$ (x = 0.3, 0.5, and 0.7) system nanoperovskite materials were successfully synthesized by the hydroxide precursor technique at a reasonably low temperature of 800 ºC. The purity was confirmed with JCPDS files of respective nanomaterials and observed splitting in X-ray diffraction patterns revealed the rhombohedrally distorted structures. The specific surface area of 20 m^2/g could be obtained for all intermediate compositions. These compounds are ESR inactive at room temperature but showed broad peaks at liquid nitrogen temperature due to spin-orbit coupling and Ni^{+3}, Co^{+3} ions are ESR inactive. A significant rise in the propylene oxidation catalytic activity is observed by the B-site substitution of Co^{+3} in the $LaNiO_3$ perovskite nanosystem. $LaCoO_3$ shows the highest activity of 96 %, whereas $LaNiO_3$ shows 92 % for propylene oxidation and has no correlation with their specific surface area. Though the specific surface areas of x = 0.3, and 0.7 compositions were highest,

having a value of 20.4 and 20.7 m^2/g, respectively, but the only x = 0.7 composition shows slightly better oxidation efficiency. The intermediate compositions show higher propylene oxidation up to 225 ºC.

References

1. M. L. Medarde and J. Condens. Matter. Phys. **9**, 1679 (1997). https://doi.org/10.1088/0953-8984/9/8/003
2. L. Chavez-Guerrero, B. Medina-Lott, R. F. Cienfugos, M. A. Garza-Navarro, R. N. Vannier A. Ringuedé, M. Hinojosa and, M. Cassir, J. Rare Earth. **33**, 277 (2015). https://doi.org/10.1016/S1002-0721(14)60415-4
3. A. A. Shah, S. Ahmad, and A. Azam, J. Magn. Magn. Mater. **494**, ID 165812 (2020). https://doi.org/10.1016/j.jmmm.2019.165812
4. J. Varignon, M. N. Grisolia, J. Iniguez, A. Bartelemy, and M. Bibes, npj Quantum Mater, **2,** 21 (2017). https://doi.org/10.1038/s41535-017-0024-9
5. S. Akhtar, M. A. Alam, and H. Ahmad, J. Sci. Res. **9**, 413 (2017). https://doi.org/10.3329/jsr.v9i4.32726
6. G. Catalan, Phase Transition, **81**, 729 (2008). https://doi.org/10.1080/01411590801992463
7. J. S. A.Carneiro, J. Williams, A. Gryko, L. P. Herrera, and E. Nikolla, ACS Catal. **10**, 516 (2020). https://doi.org/10.1021/acscatal.9b04226
8. P. R. N. Silva, A. B. Soares, and Ecletica Quimica J. **34**, 31 (2009). https://doi.org/10.1590/S0100-46702009000100005
9. I. Tepech-Carrillo, A. Escobed-Morales, A. Perez-Centeno, E. Chico-Anota, J. F. Sánchez-Ramírez, E. López-Apreza, and J. Gutiérrez-Gutiérrez, J. Nanomater. ID 6917950 (2016). https://doi.org/10.1155/2016/6917950
10. M. Ghasdi and H. Alamdari, Sensor Actuators B Chem. **148**, 478 (2010). https://doi.org/10.1016/j.snb.2010.05.056
11. R. Thakur, A. srivastava, R. Thakur, and N. K. Gaur, J. Alloy. Compds. **516**, 58 (2012). https://doi.org/10.1016/j.jallcom.2011.11.128
12. T. Seiyama, Catal. Rev. Sci. Eng. **34**, 281 (1992). https://doi.org/10.1080/01614949208016313
13. M. A. Peña and J. L. G. Fierro, Chem. Rev. **101**, 1981 (2001). https://doi.org/10.1021/cr980129f
14. G. Kremenic, J. M. L. Nieto, J. M. D. Tascon, and L. G. Tejuca, J. Chem. Soc. Faraday Trans. I **81**, 939 (1985). https://doi.org/10.1039/F19858100939
15. T. Vaz and A. V. Salker, Mat. Sci. Eng. B, **143**, 81 (2007). https://doi.org/10.1016/j.mseb.2007.07.027
16. D. Aman, T. Zaki, S. Mikhail, and S. A. Selim, Catal. Today 164, 209 (2011). https://doi.org/10.1016/j.cattod.2010.11.034
17. J. Garcia, D. Beltran, F. Sapina, and M. J. Sanches, J. Alloy Compd. **188**, 170 (1992). https://doi.org/10.1016/0925-8388(92)90668-Y
18. D. D. Agarwal and S. H. Goswami, React. Kinet. Catal. Lett. **53**, 441 (1994). https://doi.org/10.1007/BF02073053
19. R. L. Dutta and A. Syamal, Elements of Magnetochemistry, 2nd Edition (New Delhi: East-West Press) pp. 210.
20. M. Iwamoto, Y. Yoda, N. Yamazoe, and T. Seiyama, J. Phys. Chem. **82**, 2564 (1978). https://doi.org/10.1021/j100513a006
21. V. C. Corberan and L. G. Tejuca, J. Colloid Interface Sci. **129**, 270 (1989). https://doi.org/10.1016/0021-9797(89)90439-6
22. P. Salomonsson, T. Griffin, and B. Casemo, Appld. Catal. A: Gen. **104**, 175 (1993). https://doi.org/10.1016/0926-860X(93)85097-9